This document is the accepted manuscript version of the following article:
Aeppli, M., Vranic, S., Kaegi, R., Kretzschmar, R., Brown, A. R., Voegelin, A., … Sander, M. (2019). Decreases in iron oxide reducibility during microbial reductive dissolution and transformation of ferrihydrite. Environmental Science and Technology, 53(15), 8736-8746. https://doi.org/10.1021/acs.est.9b01299

Decreases in iron oxide reducibility during microbial reductive dissolution and transformation of ferrihydrite

Meret Aeppli,[†,‡] Sanja Vranic,[†] Ralf Kaegi,[‡] Ruben Kretzschmar,[†] Ashley R. Brown,[‡] Andreas Voegelin,[‡] Thomas B. Hofstetter,[*,†,‡] and Michael Sander[*,†]

Institute of Biogeochemistry and Pollutant Dynamics, ETH Zürich, 8092 Zürich, Switzerland, and Swiss Federal Institute of Aquatic Science and Technology (Eawag), 8600 Dübendorf, Switzerland

E-mail: thomas.hofstetter@eawag.ch; michael.sander@env.ethz.ch

*To whom correspondence should be addressed
[†]Institute of Biogeochemistry and Pollutant Dynamics, ETH Zürich, 8092 Zürich, Switzerland
[‡]Swiss Federal Institute of Aquatic Science and Technology (Eawag), 8600 Dübendorf, Switzerland

Abstract

Ferrous iron formed during microbial ferric iron reduction induces phase transformations of poorly crystalline into more crystalline and thermodynamically more stable iron (oxyhydr)oxides. Yet, characterizing the resulting decreases in the reactivity of the remaining oxide ferric iron toward reduction (i.e., its reducibility) has been challenging. Here, we used the reduction of six-line ferrihydrite by *Shewanella oneidensis* MR-1 as a model system to demonstrate that mediated electrochemical reduction (MER) allows directly following decreases in oxide ferric iron reducibility during the transformation of ferrihydrite into goethite and magnetite which we followed by X-ray diffraction analyses and transmission electron microscopy imaging. Ferrihydrite was fully reducible in MER at both pH_{MER} of 5.0 and 7.5. Decreases in iron oxide reducibility associated with ferrihydrite transformation into magnetite were accessible at both pH_{MER} because the formed magnetite was not reducible under either of these conditions. Conversely, decreases in iron oxide reducibility associated with goethite formation were apparent only at the highest tested pH_{MER} of 7.5 and thus the thermodynamically least favorable conditions for iron oxide reductive dissolution. The unique capability to adjust the thermodynamic boundary conditions in MER to the specific reducibility of individual iron (oxyhydr)oxides suggests that this electrochemical approach is broadly applicable for studying changes in iron oxide reducibility in heterogeneous environmental samples such as soils and sediments.

Introduction

Microbial electron transfer reactions to iron (oxyhydr)oxides (hereafter referred to as iron oxides) are central to many redox processes that control the biogeochemical cycling of elements and redox transformations of pollutants in both natural and engineered systems.[1–3] Iron-reducing microorganisms utilize oxide ferric iron (oxide-Fe^{III}) as terminal electron acceptor for anaerobic respiration of organic substrates.[4–8] These microorganisms preferentially reduce poorly crystalline iron oxides with lower thermodynamic stabilities, and hence higher reduction potentials, over crystalline iron oxides.[9–11] Ferrihydrite is among the most abundant poorly crystalline iron oxides in nature and is often used by iron-reducing microorganisms in anaerobic microbial respiration.[12,13] Yet, the ferrous iron (Fe^{II}) that forms during microbial ferrihydrite reduction can induce transformations of the unreacted ferrihydrite into thermodynamically more stable iron oxides, such as goethite and magnetite.[14–16] These transformations cause a decrease in the reactivity of the remaining oxide-Fe^{III} toward reduction as a consequence of the decreases in iron oxide reduction potentials and specific surface areas that are associated with the transformations. We will subsequently refer to the reactivity of the iron oxide toward reduction as reducibility, which we broadly define to include both the rates and extents of electron transfer to oxide-Fe^{III}. The decrease in iron oxide reducibility during phase transformations may constrain microbial respiration to the remaining oxide-Fe^{III}.[17–22] Determining decreases in iron oxide reducibility during phase transformations is therefore essential to understand biogeochemical and pollutant transformation processes that are coupled to microbial iron oxide reduction.[23–25]

The importance of microbial reductive dissolution and transformation of poorly crystalline iron oxides is well documented.[14–16,26–30] However, earlier studies primarily focused on two aspects: First, the quantification of Fe^{II} formation during microbial Fe^{III} reduction (e.g. by colorimetric assays) and second, the characterization of changes in iron oxide mineralogy (e.g., by spectroscopic techniques). While information on both aspects is critical to understand the dynamics of microbial

iron oxide reduction and the resulting phase transformations, such information does not provide direct insights into the decreases in iron oxide reducibility associated with the phase transformations. Obtaining insights into the decreases in iron oxide reducibility is challenging because reducibility assessments need to be performed on a well-defined thermodynamic basis to compare the reducibility of the initial poorly crystalline iron oxide to the reducibility of its transformation products. These different reducibilities can be detected in assessments performed over a wide range of thermodynamic boundary conditions for iron oxide reduction. However, commonly used reductive dissolution assays[31–35] provide only limited possibilities to adjust these boundary conditions because they are typically performed at a single pH and with a single reductant.

We recently introduced mediated electrochemical reduction (MER) as a novel approach to analyze iron oxide reducibility.[36,37] MER allows controlling and systematically altering the thermodynamic boundary conditions for iron oxide reduction by independently varying the pH in and the reduction potentials applied to the electrochemical cells to which iron oxide suspensions are added. The electrochemical cells contain dissolved, redox-active mediator molecules that facilitate electron transfer from the working electrodes of the cells to the added iron oxides. This electron transfer to the iron oxides results in reductive current peaks that provide direct measures of both rates and extents of oxide-Fe^{III} reduction.[38,39] Using MER, we demonstrated that the reducibilities of pure goethite and hematite can be linked to the thermodynamic driving forces for their reductive dissolution as defined by the boundary conditions in MER.[37] We subsequently showed that MER also allows following decreases in iron oxide reducibility during ferrihydrite transformation into goethite and magnetite that we induced by reacting ferrihydrite with dissolved Fe^{II}.[36] We quantitatively linked the decreases in iron oxide reducibility to concurrent phase transformations that we determined using X-ray diffraction (XRD). Based on this previous work, we hypothesize that MER is also applicable to determine changes in iron oxide reducibility during microbial ferrihydrite reduction and the resulting transformation of ferrihydrite into thermodynamically more stable iron oxides. Demonstrating this applicability is important given the key role of microbial iron oxide

reduction in many biogeochemical and pollutant transformation processes.

This work aims to establish that MER allows to directly quantify decreases in iron oxide reducibility associated with the transformation of poorly crystalline into thermodynamically more stable iron oxides induced by Fe^{II} formed during microbial Fe^{III} reduction. We used a model incubation system containing six-line ferrihydrite, the facultative anaerobic bacterium *Shewanella oneidensis* strain MR-1, and lactate as electron donor. We chose this model system because ferrihydrite reduction by *S. oneidensis* and the resulting transformation of ferrihydrite into thermodynamically more stable oxides are well studied,[15,16,26–28,30] yet electrochemical assessments of the associated changes in iron oxide reducibility remain missing. As compared to only following microbial iron oxide reduction during the incubations, the electrochemical analyses offer the advantage that (changes in) iron oxide reducibilities are assessed under well-defined thermodynamic boundary conditions that can be controlled in the electrochemical cells. The boundary conditions can further be systematically varied to characterize the reducibilities of iron oxides with very different thermodynamic stabilities. In our incubations, we systematically varied the initial lactate concentration to direct ferrihydrite transformation into different ratios of goethite and magnetite. We combined established analyses of Fe^{II} formation (quantification by the phenanthroline assay) and changes in iron oxide mineralogy (by XRD and electron microscopy (EM)) during the incubations with novel assessments of decreases in iron oxide reducibility using MER. We focused these assessments on decreases in the extents of electron transfer to oxide-Fe^{III} in MER and not the rates at which these electrons are transferred.[36] In addition to MER, we employed mediated electrochemical oxidation (MEO) to assess changes in the reactivity of Fe^{II} formed during microbial Fe^{III} reduction toward oxidation.[39,40]

Materials and Methods

Solutions and suspensions

All suspensions and solutions (see Supporting Information, Section S1 for a list of chemicals) were prepared with doubly deionized water (resistivity >18.2 MΩ·cm, Barnstead Nanopure Diamond Water Purification System). Anoxic solutions for incubations inside an anoxic glovebox (see below) were prepared by purging them with ultrahigh purity N_2 (99.999%) for at least 3 h.

Microbial Fe^{III} reduction experiments

Microbial Fe^{III} reduction experiments, collection and preparation of iron oxide suspensions for spectrophotometric analyses using the phenanthroline assay, XRD and EM analyses as well as MER and MEO were performed inside an anoxic glovebox (N_2 atmosphere, <2 ppm O_2 Unilab 2000, MBraun). Six-line ferrihydrite was synthesized[41] as described in Section S2 and was used in the incubations within 1 week of being synthesized. Bacterial cultures were prepared as described in Section S3. Incubations were conducted with resting cell cultures in a non-growth medium to limit increases in cells numbers as well as the microbial production of extracellular polymeric substances and electron shuttling compounds which would likely have resulted in more complex Fe^{II}-induced mineral transformations. Prior to use, all glassware was autoclaved (Zirbus Technology, LTA 2x3x4) and pH-buffered solutions were filter-sterilized (0.22 μm polyethersulfone syringe filters, TPP). Incubations were carried out in duplicate 100 mL glass vials that were sealed with butyl rubber stoppers and crimped with aluminium caps. The crimped incubation vials were autoclaved and subsequently flushed with ultrahigh purity N_2 (99.999%) through sterile filters (0.22 μm polyethersulfone syringe filters, TPP). Incubation vials were filled with sterile solutions buffered to pH 7.00 (0.03 M 3-(*N*-morpholino)propanesulfonic acid (MOPS), 0.01 M NaCl) that contained varying lactate concentrations of 0.078, 0.30, 1.25, 5.00 or 20.00 mM. Ferrihydrite suspensions

were added to the incubation vials to an initial Fe^{III} concentration of 5.0 mM. Microbial incubations were thus started at varying initial electron donor-to-acceptor ratios (lactate:Fe^{III}) of 1:16, 1:4, 1:1:, 4:1, and 16:1 electron equivalents, assuming that *S. oneidensis* oxidized lactate to acetate and thus transferred four electrons per lactate molecule to oxide-Fe^{III}. We chose these ratios based on previous studies[15,16,26–28,30] to direct ferrihydrite transformation into goethite (at low ratios and hence lower initial Fe^{II} formation rates) and magnetite (at high ratios and hence higher initial Fe^{II} formation rates). We did not assess potential microbial production of extracellular polymeric substances and electron shuttling compounds during the incubations and we did not elucidate by which pathway electrons were transferred from *S. oneidensis* to the oxides because these analyses would have been outside the scope of our work.

Microbial reduction of ferrihydrite was initiated by the addition of suspended *S. oneidensis* cells to the incubation vials to concentrations of $\approx 2.2 \cdot 10^8$ cells mL^{-1}. The inoculated incubation vials were rotated at 20 rpm on an overhead shaker (Reax 2, Heidolph) for the duration of the incubations (up to 36 d) at 25±2°C. At multiple time points during the incubations, 7.0 mL iron oxide suspension aliquots were collected from the sealed incubation vials through sterile needles into disposable plastic syringes. Duplicate vials for a given donor-to-acceptor ratio were sampled in an alternating pattern. The time points at which the individual vials were analyzed therefore varied between the duplicates. On the collected aliquots, we conduced the following analyses: 1. We quantified $Fe_{total,\ phen}$ and Fe^{II}_{phen} concentrations using the phenanthroline (phen) assay (after dissolution of the iron oxides in 3 M HCl)[42,43] and calculated Fe^{III}_{phen} concentrations by subtracting Fe^{II}_{phen} from $Fe_{total,\ phen}$ concentrations. 2. We determined the mineralogy and morphology of the iron oxides by XRD and EM (see below). 3. We quantified the extents to which electrons were transferred to oxide-Fe^{III} and from Fe^{II} using MER and MEO, respectively (see below). Incubations were terminated once microbial iron oxide reduction had ceased and mineralogical transformations had stopped. Sterile control vials containing ferrihydrite but no *S. oneidensis* cells showed no mineral transformation, no formation of Fe^{II}, and no changes in the reducibility of oxide-Fe^{III}

over 552 h (Section S4). We performed additional incubations with bicarbonate and piperazine-1,4-bis(2-ethanesulfonic acid) buffers instead of MOPS buffer and summarize the results of these incubations in Section S5.

X-ray diffraction analysis

The solids in the collected 7.0 mL aliquots were analyzed by XRD, as described in Aeppli et al.[36] and Section S6. X-ray diffractograms were recorded (D8 Advance, Bruker) from 10 to 70°2θ (step size 0.02°2θ and 6 or 10 s acquisition time per step) in Bragg-Brentano geometry using Cu Kα radiation (λ =1.5418 Å, 40 kV and 40 mA) and a high-resolution energy-dispersive 1-D detector (LYNXEYE). The identities of the transformation products and the mass fractions of all Fe phases in each aliquot were determined by Rietveld quantitative phase analysis (TOPAS Version 5, Bruker) using a hkl-phase for ferrihydrite calibrated according to the partial or no known crystal structure (PONKCS) method[36,44,45] and published structure files for goethite, magnetite, siderite and lepidocrocite.

Electron microscopy

We investigated the iron oxides in the collected 7.0 mL aliquots on a dedicated scanning transmission electron microscope (STEM, 2700Cs, Hitachi) operated at an acceleration voltage of 200 kV, as described in Aeppli et al.[36] and Section S7. Images were recorded using a secondary electron or high angular annular dark field detector.

Mediated electrochemical analyses

We used MER and MEO to characterize changes in the reactivities of Fe^{III} toward reduction and Fe^{II} toward oxidation, respectively, over the course of the microbial Fe^{III} reduction experiments. MER and MEO measurements were conducted using two eight-channel potentiostats (models

1000B and 1000C, CH Instruments) operated in chronoamperometric mode[37,38]. The setup of the electrochemical cells is described in Section S8. The reduction potentials applied to the working electrodes (WEs) of MER and MEO cells were measured against Ag/AgCl reference electrodes (Re1B, ALS) but are reported herein versus the standard hydrogen electrode (E_H^{MER} and E_H^{MEO}).

MER and MEO analyses of each sample were conducted on duplicate electrochemical cells according to the following procedure. First, pH-buffered solutions were added to the WE cylinders. MER measurements were performed at pH_{MER}=5.0 (0.01 M acetate and 0.01 M KCl), 7.0 and 7.5 (both 0.01 M MOPS and 0.01 M KCl), all at applied reduction potentials of E_H^{MER}=−0.35V. We chose these MER conditions based on our previous work,[36] in which we demonstrated that these conditions allow assessing the loss of oxide-Fe^{III} reducibility upon ferrihydrite transformation into goethite and magnetite. We note that the primary motivation behind choosing these MER conditions was to characterize oxide-Fe^{III} reducibility and not to closely mimic (pH) conditions typically encountered during iron oxide reduction in natural soils.[36] MEO measurements were performed at pH_{MEO}=5.0 (0.01 M acetate and 0.01 M KCl) and an applied oxidation potential of E_H^{MEO}=+0.79V. MER and MEO measurements were initiated by applying E_H^{MER} and E_H^{MEO} to MER and MEO cells, respectively. Once stable background currents were obtained, we added the mediators diquat (1,1′-ethylene−2,2′-bipyridil, standard reduction potential E_H^0=−0.35 V) to MER cells and ABTS (2,2′-azino-bis(3-ethylbenzothiazoline-6-sulfonic acid), E_H^0=+0.70 V) to MEO cells (both from 10 mM stock solutions). Diquat reduction in the MER and ABTS oxidation in the MEO cells resulted in reductive and oxidative current peaks, respectively. When currents had returned to baseline values, the concentrations of reduced diquat in the MER and oxidized ABTS in the MEO cells were 0.255 mM and 0.251 mM, respectively. We calculated these values with the Nernst equation using the volumes and concentrations of mediator stock solutions that we added to the electrochemical cells and the published standard reduction potentials of the two mediators. At this point, 50 μL of the iron oxide suspensions in the 7.0 mL aliquots collected from the incubation vials (see above) were pipette-transferred into each MER and MEO cell. Mediated

reduction of oxide-Fe^{III} in MER and mediated oxidation of oxide-associated and dissolved Fe^{II} in MEO resulted in reductive and oxidative current peaks, respectively. MER and MEO measurements were terminated when currents re-attained the baseline values measured prior to the addition of the iron oxide suspensions to the electrochemical cells.

Herein, we discuss iron oxide reducibility in terms of the extents of electron transfer to oxide-Fe^{III} under defined MER conditions despite the fact that reduction rates were more susceptible than reduction extents to changes in iron oxide mineralogy during ferrihydrite transformation in our previous study.[36] However, the analysis of rates had larger uncertainties than the analysis of extents and these uncertainties were particularly pronounced for samples that had been extensively reduced by *S. oneidensis* and hence had small current responses in MER.

We determined the moles of electrons transferred from the WE to oxide-Fe^{III} in MER and hence the moles of Fe^{III} atoms reduced, $n_{Fe^{III}_{MER}}$ ($mol_{Fe^{III}}$), by integration of reductive current peaks in response to adding iron oxide suspensions to the MER cells (eq. 1).

$$n_{Fe^{III}_{MER}} = \frac{1}{F}\int_{t_0}^{t_{end}} I_{MER}\, dt \tag{1}$$

where I_{MER} is the baseline-corrected reductive current (A), F is the Faraday constant, and t_0 and t_{end} (s) denote the initial and final integration boundaries for each reductive current peak. We analogously determined the moles of oxide-associated and dissolved Fe^{II} atoms that were oxidized in MEO, $n_{Fe^{II}_{MEO}}$ ($mol_{Fe^{II}}$), by integration of oxidative current peaks (eq. 2).

$$n_{Fe^{II}_{MEO}} = \frac{1}{F}\int_{t_0}^{t_{end}} -I_{MEO}\, dt \tag{2}$$

where I_{MEO} is the baseline-corrected oxidative current (A). We divided $n_{Fe^{III}_{MER}}$ and $n_{Fe^{II}_{MEO}}$ by the volume of iron oxide suspension added to the electrochemical cells (50 μL) to obtain concentrations of Fe^{III} reduced in MER (Fe^{III}_{MER}) and Fe^{II} oxidized in MEO (Fe^{II}_{MEO}). Baseline subtraction and peak

integration were performed using Matlab (MathWorks, code see Section S9). Error bars represent deviations of single measurements from the mean of duplicate electrochemical measurements. We report extents of Fe^{III} reduction in MER as fractions of the total Fe^{III} concentrations present in the incubation vials at the time of sample collection as quantified by the phenanthroline assay, i.e. $Fe^{III}_{MER}/Fe^{III}_{phen}$. This ratio theoretically varies between 0 (none of the Fe^{III} was reducible in MER) and 1 (all Fe^{III} was reducible in MER). For selected sampling points during the incubations, we collected only MER and MEO but no phenanthroline data (this was the case for about one fifth of all sampling points). For these sampling points, we linearly interpolated Fe^{III}_{phen} concentrations from the Fe^{III}_{phen} concentrations measured at the preceding and subsequent sampling point.

Results and discussion

Microbial Fe^{III} reduction

We performed incubations of six-line ferrihydrite with resting cells of *S. oneidensis* MR-1 at electron donor-to-acceptor ratios (lactate:Fe^{III}) from 1:16 to 16:1 electron equivalents. Figure 1a-c show changes in the concentrations of $Fe_{total,\ phen}$, Fe^{II}_{phen} (both determined with the phenanthroline assay) and the resulting calculated Fe^{III}_{phen} over the course of the incubations at donor-to-acceptor ratios of 1:16 (panel a), 1:1 (panel b) and 16:1 (panel c). Results of additional incubations at the intermediate donor-to-acceptor ratios of 1:4 and 4:1 are presented in Section S10. At all donor-to-acceptor ratios, the concentrations of $Fe_{total,\ phen}$ remained approximately constant at 5.0 mM throughout the incubations, implying that the phenanthroline assay always accounted for all iron initially added to the incubation vials. The concentrations of Fe^{II}_{phen} increased and the calculated concentrations of Fe^{III}_{phen} decreased over the course of all incubations, demonstrating that *S. oneidensis* reduced oxide-Fe^{III}. The rates and extents of microbial Fe^{III} reduction increased as the donor-to-acceptor ratio was increased from 1:16 (Figure 1a) to 16:1 (Figure 1c), in line with

previous studies.[15,16,26]

In incubations with donor-to-acceptor ratios of 1:16 and 1:4 (Figures 1a and S15a), the concentrations of Fe^{II} that had formed by the end of the incubations were in good agreement with the maximum possible Fe^{II} concentrations that we calculated based on the assumption that all added lactate was oxidized to acetate and the reducing equivalents liberated in this oxidation were transferred to oxide-Fe^{III} (Section S11). These observations thus suggest that microbial iron oxide reduction in these incubations ceased when the electron donor lactate was completely consumed. In incubations with donor-to-acceptor ratios of 1:1 and above (Figures 1b,c and S15b), microbial reduction of oxide-Fe^{III} remained incomplete at the end of the incubations despite stoichiometric or even excess reducing equivalents in lactate relative to Fe^{III} (Section S11). Microbial respiration in these incubations therefore likely ceased as a result of decreasing iron oxide reducibility, as detailed below. Although not explicitly tested, we consider it less likely that reduction ceased because of microbial cell death given that previous work showed that resting cells of *Shewanella putrefaciens* CN32 were capable of reducing Fe^{III} in clay minerals beyond 30 d of incubation.[46,47]

Iron oxide transformations during microbial Fe^{III} reduction

We determined changes in iron oxide mineralogy and morphology during microbial Fe^{III} reduction by XRD and EM analyses. In all incubations, goethite and magnetite were the main products of ferrihydrite transformation. By comparison, the formation of both crystalline siderite and lepidocrocite was minor (final mass fractions smaller than 1%) and is thus not further discussed. Figure 1d-f show the temporal changes in the molar fractions of Fe^{III} in ferrihydrite, goethite and magnetite over the course of the incubations. Figure 1g-i show EM images of iron oxides collected toward the end of the incubations when microbial iron oxide reduction had leveled off. Additional EM images of iron oxides sampled over the course of the incubations are presented in Section S12. We observed good agreement between iron oxide mineralogy determined by XRD and iron oxide morphologies apparent from EM images.

At the lowest donor-to-acceptor ratio of 1:16 (Figure 1d), ferrihydrite exclusively transformed into goethite with 96% of oxide-Fe^{III} being present as goethite after 516 h. Goethite formation was confirmed by the EM image which shows goethite needles with lengths and widths of 60-600 nm and 10-50 nm, respectively (Figure 1g). We ascribe the formation of goethite to low concentration ratios of formed Fe^{II} to oxide-Fe^{III} in this incubation. Such low ratios presumably resulted in low concentrations of ferrihydrite-associated Fe^{II} that are known to catalyze its transformation into goethite through a dissolution-reprecipitation mechanism.[12,14,15,26,27,30,36]

At donor-to-acceptor ratio of 1:1 (Figure 1e), ferrihydrite transformed into a final mixture of 32% goethite-Fe^{III} and 62% magnetite-Fe^{III} (6% unreacted ferrihydrite). The EM image in Figure 1h shows goethite needles (lengths and widths of up to 100 nm and ≈ 10 nm, respectively) in close association with diamond-shaped magnetite particles (diameters of 80-300 nm; in agreement with crystallite sizes of ≈ 177 nm that we estimated from the X-ray diffractograms in Figure S13a). Magnetite formation was not continuous over the course of the incubation (Figure 1e): In an initial phase (< 120 h), only goethite formed. After this initial phase, magnetite formed over a relatively short time span from 120 to 290 h, which is depicted by the vertical grey bar in Figure 1e. Magnetite formed at the expense of both ferrihydrite and goethite, as previously reported.[14]

Transformation of ferrihydrite into magnetite became more extensive as the donor-to-acceptor ratio increased from 1:4 to 4:1 (Figures 1e, S16 and Section S11). This trend was consistent with increasing concentration ratios of Fe^{II} to oxide-Fe^{III},[15,16,28,30,36] which presumably resulted in higher concentrations of ferrihydrite-associated Fe^{II}. This associated Fe^{II} is known to favor solid state conversion of ferrihydrite into magnetite.[48,49] The magnetite that formed in these incubations had close to stoichiometric ratios of structural Fe^{III}:Fe^{II} of 1:(0.51±0.02), as determined from the X-ray diffractograms[50] (Section S13).

At the highest donor-to-acceptor ratio of 16:1 (Figure 1f), we observed incomplete ferrihydrite transformation: 47% of oxide-Fe^{III} were still present as ferrihydrite at the end of the experiment (particles with diameters of ≈ 5 nm in the EM image in Figure 1i). Goethite was the dominant

transformation product under these conditions, making up 47% of the oxide-Fe^{III}. The EM image shows that formed goethite needles had lengths of up to 30 nm and widths of ≈ 5 nm (Figure 1i). These goethite needles were considerably smaller than those formed at the donor-to-acceptor ratio of 1:16, as evident from the EM images (Figure 1i,g) and the crystallite sizes that we estimated from X-ray diffractograms (3 and 13 nm, respectively, Figures S14 and S12a). While the high final Fe^{II} concentrations (> 3 mM) in this experiment should favor ferrihydrite transformation into magnetite over goethite, only very small amounts of magnetite formed (i.e., 7% of oxide-Fe^{III} were present as magnetite at the end of the incubation). We speculate that the high lactate concentrations (initial concentrations of 20 mM) disfavored magnetite formation through adsorption of lactate onto the ferrihydrite surface and that this lactate adsorption suppressed Fe^{2+} adsorption and thus electron transfer from Fe^{2+} to ferrihydrite-Fe^{III}, a key step in the transformation of ferrihydrite into magnetite.[30,51,52]

Decreases in iron oxide reducibility during microbial Fe^{III} reduction

Mediated electrochemical reduction and oxidation at $pH_{MER} = pH_{MEO} = 5.0$

Figure 2a-c show selected current responses obtained in MER (red traces) and MEO (blue traces) at $pH_{MER} = pH_{MEO} = 5.0$ of iron oxide suspensions collected at the beginning, during, and at the end of the incubations at donor-to-acceptor ratios of 1:16, 1:1 and 16:1. Figure 2d-f show the concentrations of Fe^{III} reduced in MER (Fe^{III}_{MER}) and Fe^{II} oxidized in MEO (Fe^{II}_{MEO}) that we calculated from the reductive (eq. 1) and oxidative (eq. 2) current responses, respectively. We compare these concentrations to the concentrations of Fe^{III}_{phen} and Fe^{II}_{phen} determined by the phenanthroline assay (semi-transparent symbols in Figures 2d-f; replotted from Figure 1a-c).

Incubations with ferrihydrite transformation into goethite. During incubations at donor-to-acceptor ratios of 1:16 and 16:1 that led to ferrihydrite transformation into goethite (Figure 1d,f), the areas of current peaks decreased in MER and increased in MEO (Figure 2a,c). These changes solely

reflected microbial Fe^{III} reduction: over the entire course of the incubations, the concentrations of Fe^{III}_{MER} and Fe^{II}_{MEO} were in very good agreement with the corresponding concentrations determined with the phenanthroline assay (Figure 2d,f). All Fe^{III} and Fe^{II} was therefore detected in MER and MEO, respectively. We conclude that the thermodynamic boundary conditions in MER and MEO at $pH_{MER} = pH_{MEO} = 5.0$ were sufficiently reducing and oxidizing, respectively, to result in complete reduction of Fe^{III} in ferrihydrite and goethite and complete oxidation of Fe^{II} that was dissolved or adsorbed to the ferrihydrite and goethite surfaces.

Incubations with ferrihydrite transformation into goethite-magnetite mixtures. In incubations with ferrihydrite transformation into goethite-magnetite mixtures (at donor-to-acceptor ratio of 1:1), MER peak areas decreased and MEO peak areas concurrently increased during the first phase of the incubation at < 120 h (Figure 2b) when ferrihydrite transformed into goethite (Figure 1e). In this first phase, the concentrations of Fe^{III}_{MER} and Fe^{II}_{MEO} matched the corresponding concentrations determined with the phenanthroline assay. Similar to the two incubations discussed above, this finding again implies that all Fe^{III} in ferrihydrite and goethite was reducible in MER and all dissolved and adsorbed Fe^{II} was oxidizable in MEO. During the first phase of the incubation, changes in the current responses in MER and MEO therefore solely reflected microbial Fe^{III} reduction. Upon magnetite formation in the second phase of the incubation between 120 and 290 h, not only MER but also MEO peak areas decreased (Figure 2b) and the concentrations of Fe^{III}_{MER} and Fe^{II}_{MEO} were lower than the concentrations determined with the phenanthroline assay (Figure 2e). These results imply that the reactivities of Fe^{III} toward reduction and Fe^{II} toward oxidation decreased during magnetite formation: structural Fe^{III} and Fe^{II} in magnetite were therefore not or only partially reducible and oxidizable in MER and MEO, respectively. We note that these changes in the reactivities of oxide-Fe^{III} and Fe^{II} would have gone unnoticed had only the phenanthroline and XRD data been available.

We assessed what fraction of the Fe^{III} in magnetite was reducible in MER: For the iron oxide suspensions collected at the end of the incubation, we would have expected a reducible concentration

of Fe^{III}_{MER} of 0.96±0.02 mM, assuming that all goethite-Fe^{III} in the mixture (32% of oxide-Fe^{III}, Figure 1e) but none of the magnetite-Fe^{III} had been reducible. This calculated concentration is higher than the measured concentration of Fe^{III}_{MER} = 0.61±0.11 mM, implying that none of the Fe^{III} in magnetite was reducible and that only part of the Fe^{III} in goethite was reducible. The goethite in the goethite-magnetite mixture obtained at the end of the incubation was thus less reducible than the goethite that had formed on the onset of the incubation at < 120 h.

We also assessed the fraction of total Fe^{II} in magnetite that was oxidizable in MEO at the end of the incubation. For this assessment, we first calculated the concentration of Fe^{II} in magnetite. To this end, we estimated the concentration of Fe^{III} in magnetite by multiplying the total Fe^{III}_{phen} concentration (3.0±0.02 mM, Figure 1b) by the molar fraction of total Fe^{III} that was present in magnetite (0.62, Figure 1e). We estimated a concentration of Fe^{II} in magnetite of 0.98 ± 0.03 mM by multiplying the concentration of Fe^{III} in magnetite with the ratio of Fe^{II} to Fe^{III} in magnetite (0.52, Figure S21b). Second, we calculated a concentration of Fe^{II} that was not oxidizable in MEO of 0.64±0.11 mM by subtracting Fe^{II}_{MEO} (1.26±0.01 mM, Figure 2e) from Fe^{II}_{phen} (1.90±0.11 mM, Figure 1b). The concentration of Fe^{II} that was oxidizable in MEO was thus smaller than the concentration of Fe^{II} in magnetite (0.98 ± 0.03 mM). Hence, only a fraction (around 65%) but not all of the the structural Fe^{II} in magnetite was oxidizable in MEO.

The biogenic magnetite formed herein was not reducible at pH_{MER} = 5.0, whereas abiotically formed magnetite that we previously analyzed was fully reducible under the same MER conditions.[36] This lower reducibility of the biogenic than the abiotically formed magnetite likely resulted from a combination of factors, including differences in the morphology and stoichiometry of the magnetites, as discussed below, as well as differences in magnetite surface accessibility caused by coatings of other minerals on the magnetite surface. EM images revealed that the biogenic magnetite was larger (diameters of 80-300 nm, EM images in Figure S20e,f) than the abiotically formed magnetite (diameters of 10-30 nm, EM images in Figures S23 and S24 in Aeppli et al.[36]). These particle sizes were in good agreement with crystallite sizes that we estimated based on the X-ray

diffractograms (i.e., 117 nm for biogenic magnetite (Figure S13a) and only 15 nm for abiotically produced magnetite (Figure S11a,b in Aeppli et al.[36])). The biogenic magnetite had a close to stoichiometric ratio of structural Fe^{III}:Fe^{II} of 1:0.52 (Figure S21b) as compared to the abiotically formed magnetite which was understoichiometric (structural Fe^{III}:Fe^{II} of 1:0.37, Figure S16a,b in Aeppli et al.[36]). The higher stoichiometry of the biogenic magnetite implies that it had a lower reduction potential than the abiotically formed magnetite.[53–55] We note that previous studies also observed closer to stoichiometric ratios of structural Fe^{III}:Fe^{II} for biogenic than abiotically formed magnetite.[56–58] Our finding that variations in the morphological and mineralogical properties of a given mineral (here biogenic versus abiotically produced magnetite) largely alter the reducibility of oxide-Fe^{III} highlights the need for MER because such reactivity differences cannot be inferred from spectroscopic and microscopic analyses alone.

Mediated electrochemical reduction at pH_{MER} = 7.5

To determine decreases in iron oxide reducibility associated not only with the transformation of ferrihydrite into magnetite (which was apparent in the MER analyses at pH_{MER} = 5.0) but also of ferrihydrite transformation into goethite, we analyzed the same iron oxide suspensions also at higher pH_{MER} of 7.5 and thus at smaller thermodynamic driving force for iron oxide reductive dissolution. Figure 3a-c show selected reductive current responses obtained in MER at pH_{MER} = 7.5 of iron oxide suspensions collected over the course of the incubations. For direct comparison, we replotted current responses obtained on the same iron oxide suspensions during analysis at pH_{MER} = 5.0 (see Figure 2a-c). The reductive current responses obtained at pH_{MER} = 7.0 lay in between the responses obtained at pH_{MER} = 7.5 and 5.0 (Section S14). We assessed iron oxide reducibility in terms of the extents of Fe^{III} reduction in MER, as presented in Figure 3d-f in the form of Fe^{III} reducible in MER relative to Fe^{III}_{phen} (i.e., $Fe^{III}_{MER}/Fe^{III}_{phen}$).

Incubations with ferrihydrite transformation into goethite. All iron oxide suspensions collected from incubations in which ferrihydrite preferentially transformed into goethite (i.e., at donor-to-

acceptor ratios of 1:16 and 16:1) showed reductive current peaks at pH_{MER} = 7.5, implying that at least part of the oxide-Fe^{III} remained reducible under these conditions (Figure 3a,c). Integration of the reductive current peaks revealed that Fe^{III} in suspensions collected at the onset of the incubations (when Fe^{III} was present primarily in the form of ferrihydrite) was fully reducible. With increasing ferrihydrite transformation into goethite, however, iron oxide reducibility decreased. At the end of the incubations, only about 50% - 60% of the Fe^{III} was reducible (i.e., $Fe^{III}_{MER}/Fe^{III}_{phen}$ = 0.48±0.01 after 503 h, Figure 3d and 0.57±0.02 after 856 h, Figure 3f). The lower reducibility of oxide-Fe^{III} at pH_{MER} = 7.5 than pH_{MER} = 5.0 was consistent with the smaller thermodynamic driving force for goethite reductive dissolution at the higher pH_{MER}: Using a standard reduction potential, E^0_H, for goethite of 0.768 V,[59] we estimated that the increase in pH_{MER} from 5.0 to 7.5 (at E^{MER}_H = −0.35 V) lowered the reaction driving force, $\Delta_r G$, for the reductive dissolution of goethite from −47 to −4 kJ per mole of transferred electrons (Section S15). Our observation of incomplete goethite reduction at $\Delta_r G$ = −4 kJ mol^{-1} was in good agreement with our previous work in which we showed that the extents of goethite reduction in MER decreased from fully reducible to non-reactive when $\Delta_r G$ increased from −20 to −7 kJ mol^{-1}.[37] By comparison, $\Delta_r G$ values for the reductive dissolution of ferrihydrite remained strongly negative even at pH_{MER} = 7.5 (i.e., $\Delta_r G$ = −25 kJ mol^{-1} at pH_{MER} = 7.5 in comparison to −68 kJ mol^{-1} at pH_{MER} = 5.0; as estimated based on an assumed E^0_H of ferrihydrite of 0.98 V[60]). Ferrihydrite thus remained fully reducible at the higher pH_{MER}, as shown for ferrihydrite suspensions collected at the onset of the incubations (Figure 3a,c).

Incubations with ferrihydrite transformation into goethite-magnetite mixtures. During ferrihydrite transformation into goethite-magnetite mixtures (i.e., at donor-to-acceptor ratio of 1:1, Figure 3e, reductive current responses in Figure 3b), iron oxide reducibility decreased at pH_{MER} = 7.5 during the first phase of the incubation at < 120 h when ferrihydrite transformed into goethite. Only about 66% of the Fe^{III} in the suspensions collected at the end of the first phase at 120 h were reducible in MER. Iron oxide reducibility subsequently decreased further between 120 and 290 h, concurrent with magnetite formation. At the end of the incubation, only about 15% of the Fe^{III} in

411 the collected suspensions were reducible in MER. We ascribe the decrease in iron oxide reducibility
412 during the second phase of the incubation to the formation of structural Fe^{III} in magnetite that was
413 not reducible at pH_{MER} = 7.5 given that it also was not reducible at pH_{MER} = 5.0.

414 Combining microbial Fe^{III} reduction, iron oxide transformations and de-
415 creases in iron oxide reducibility

416 Figure 4a shows the complementary information obtained from analyses of microbial Fe^{III} reduction,
417 iron oxide phase transformations, and decreases in iron oxide reducibility for the incubation at
418 donor-to-acceptor ratio of 1:1. We replotted changes in the concentration of Fe^{II}_{phen} (blue dotted
419 line, right y axis), oxide-Fe^{III} phase fractions (as % of remaining Fe^{III}) (colored stacked bars) and
420 the reducibility of the remaining oxide-Fe^{III} in MER (red solid and dashed lines for pH_{MER} = 5.0 and
421 7.5, respectively, left y axis). The bars depicting oxide-Fe^{III} phase fractions are stacked in the order
422 of decreasing reducibility in MER, as measured herein, with ferrihydrite at the bottom, followed by
423 goethite and magnetite on top. The decrease in iron oxide reducibility at pH_{MER} = 5.0 concurred
424 with magnetite formation (i.e., the red solid line decreases in parallel to the summed heights of the
425 ferrihydrite and goethite bars in Figure 4a). At pH_{MER} = 7.5, the decrease in iron oxide reducibility
426 was more pronounced than at pH_{MER} = 5.0 due to the lower reducibility of goethite at this higher
427 pH_{MER} (i.e., the red dashed line for pH_{MER}= 7.5 is closer to the ferrihydrite bars than the red solid
428 line for pH_{MER} = 5.0 in Figure 4a). The finding that magnetite was not electrochemically reducible
429 at either pH_{MER} and goethite was only partially reducible at pH_{MER} = 7.5 despite the low E_H^{MER} of
430 −0.35 V suggests that *S. oneidensis* was unable of respiring to these oxides given that respiration of
431 this organism was reported to stall already at much higher reduction potentials of −0.24 to −0.20
432 V.[61,62] We note that microbial iron oxide reduction ceased at approximately the same time at which
433 the electrochemical reducibility decreased considerably. Based on this observation we propose that
434 future studies more systematically assess the degree to which decreases in iron oxide reducibility

constrain microbial iron oxide reduction.

Implications

This work demonstrates that MER allows determining decreases in iron oxide reducibility during the microbial reductive dissolution and transformation of ferrihydrite into goethite and magnetite. Information on iron oxide reducibility obtained by MER complements traditionally employed analyses of microbial Fe^{III} reduction and iron oxide transformations. In MER, decreases in iron oxide reducibility can be assessed over a wide range of thermodynamic boundary conditions for iron oxide reduction that can be specifically adapted to the reducibilities of the iron oxides of interest, as illustrated in the schematic Figure 4b: The poorly crystalline starting phase (green) is highly reducible over the entire range of thermodynamic boundary conditions for iron oxide reduction, which is adjusted through variations in pH_{MER} (as shown herein) or E_H^{MER}. In contrast, the crystalline transformation product or mixtures of such products (orange) exhibit lower reducibilities, as becomes apparent in MER at higher pH_{MER} or E_H^{MER}.

We propose that MER could be used in future studies to assess the relative importance of two main factors that have been postulated to control rates and final extents of microbial iron oxide reductions that are coupled to phase transformations: the increase in iron oxide thermodynamic stability [17,18,20] and the decrease in the iron oxide specific surface area, [19,21,22] that result from the phase transformations. While MER can only measure the combined effects of both factors on Fe^{III} reducibility, future work could additionally follow decreases in iron oxide specific surface area during the transformations. This information would make it possible to determine the relative effects of the two factors on microbial iron oxide reduction. Furthermore, we expect that the unique feature of MER to adjust the thermodynamic boundary conditions for iron oxide reduction renders MER a widely applicable approach to assess the effects of diverse system variables on iron oxide reducibility. These variables include, but are not limited to, the presence of adsorbed inorganic and organic species on the iron oxide surface [15,63] as well as the substitution of iron in the oxide

structure by other metals.[12,64,65]

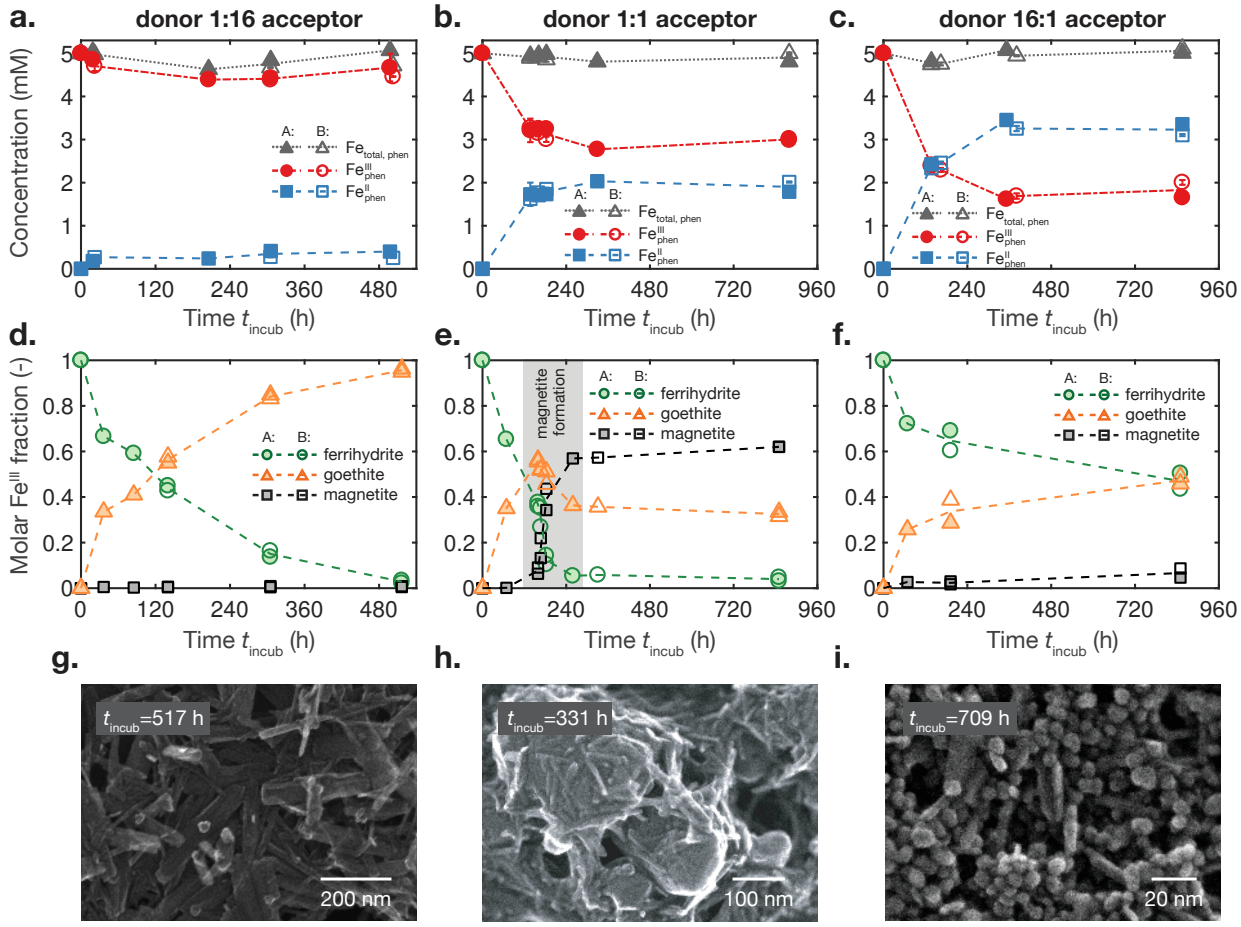

Figure 1. Iron oxide reduction by *S. oneidensis* MR-1 at varying initial concentrations of the electron donor lactate. Incubations were performed with 5.0 mM initial ferrihydrite-Fe^{III} and at initial donor-to-acceptor ratios in electron equivalents of 1:16 (0.078 mM lactate, panels a., d., g.), 1:1 (1.25 mM lactate, panels b., e., h.), and 16:1 (20.0 mM lactate, panels c., f., i.). Results are shown for duplicate incubation vials (A and B in filled and open symbols, respectively). **a.-c.** Changes in the concentrations of ferric iron (Fe^{III}_{phen}, red circles), ferrous iron (Fe^{II}_{phen}, blue squares) and total iron ($Fe_{total, phen}$, grey triangles) during the incubations, as determined with the phenanthroline assay (phen). Note that Fe^{III}_{phen} was calculated by subtracting Fe^{II}_{phen} from $Fe_{total, phen}$. **d.-f.** Changes in the molar Fe^{III} fractions in ferrihydrite, goethite and magnetite during the incubations, as determined by X-ray diffraction. The mass fractions of crystalline siderite and lepidocrocite were <1.1% in all samples and are thus not shown. Molar Fe^{III} fractions were determined from iron oxide mass fractions as described in Aeppli et al.[36]. The vertical grey bar in panel e. depicts the time span of magnetite formation. **g.-i.** Selected electron microscopy images of iron oxides collected at late stages of the incubations (as specified on the images). Images were recorded using a secondary electron detector. Lines in panels a.-f. serve as visual guides.

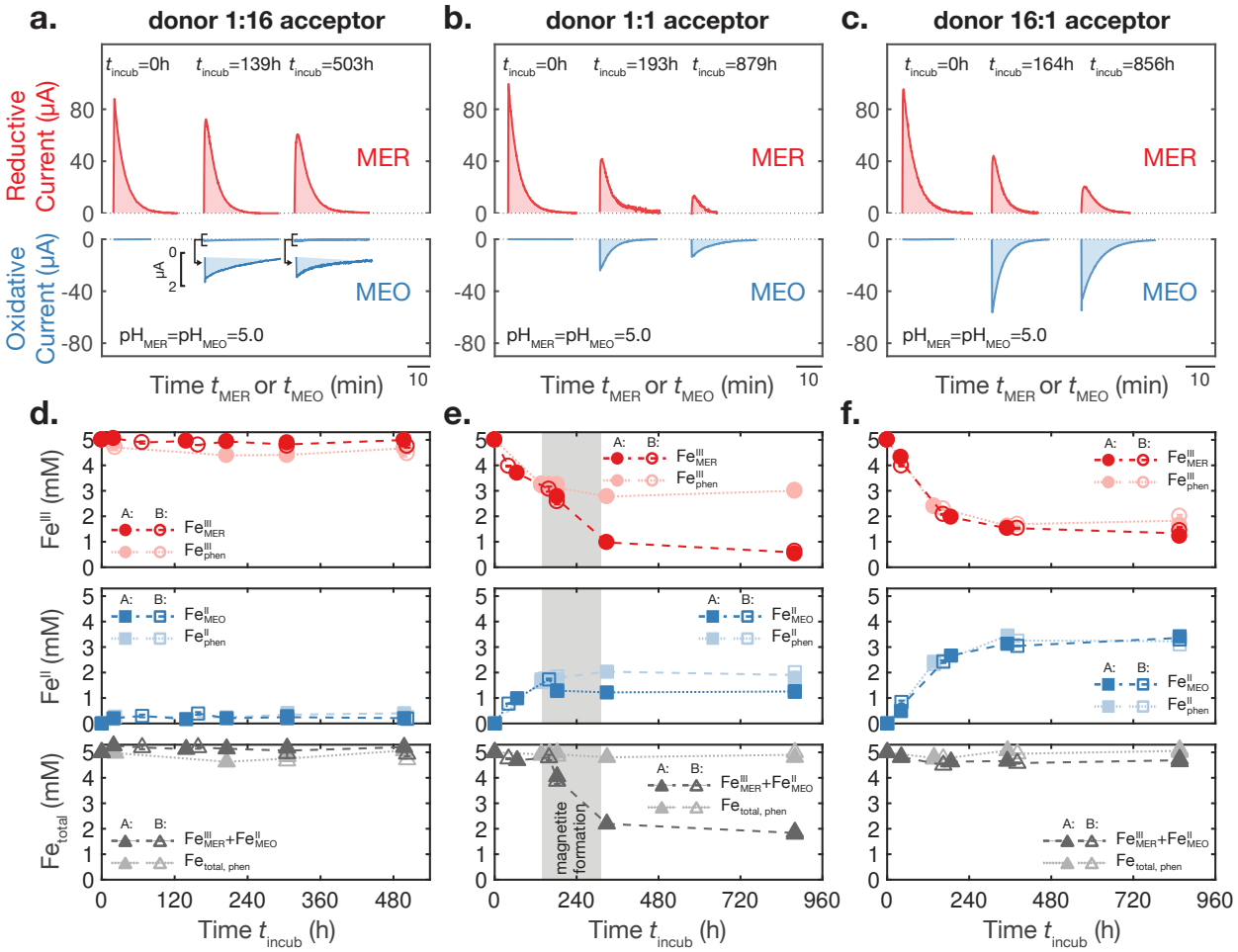

Figure 2. Changes in the reactivities of Fe^{III} and Fe^{II} over the course of the incubations as assessed by mediated electrochemical reduction (MER) and oxidation (MEO), respectively. Incubations were performed with 5.0 mM initial ferrihydrite-Fe^{III} and at initial electron donor-to-acceptor ratios in electron equivalents of 1:16 (panels a., d.), 1:1 (panels b., e.), and 16:1 (panels c., f.). Results are shown for duplicate incubation vials (A and B in filled and open symbols, respectively). **a.-c.** Selected reductive and oxidative current peaks obtained during MER (red) and MEO (blue) of iron oxide suspensions collected from the incubation vials at the beginning, at an intermediate time, and toward the end of the incubations, as specified on the plots. The x axis labels t_{MER} and t_{MEO} refer to the time (min) during MER and MEO measurements, respectively. The horizontal scale bar next to the axis label depicts a time span of 10 min. MER and MEO measurements were performed at pH_{MER} = pH_{MEO} = 5.0 and applied reduction potentials of E_H^{MER} = −0.35 V and E_H^{MEO} = +0.79 V, respectively. **d.-f.** Changes in the concentrations of Fe^{III} reduced in MER (Fe^{III}_{MER}, red circles) and Fe^{II} oxidized in MEO (Fe^{II}_{MEO}, blue squares) during the incubations as determined in MER and MEO, respectively. The sums of Fe^{III}_{MER} and Fe^{II}_{MEO} are shown as grey triangles. The iron concentrations determined with the phenanthroline assay are replotted from Figure 1a-c (semi-transparent symbols). The vertical grey bar in panel e. depicts the time span of magnetite formation. Lines in panels d.-f. serve as visual guides.

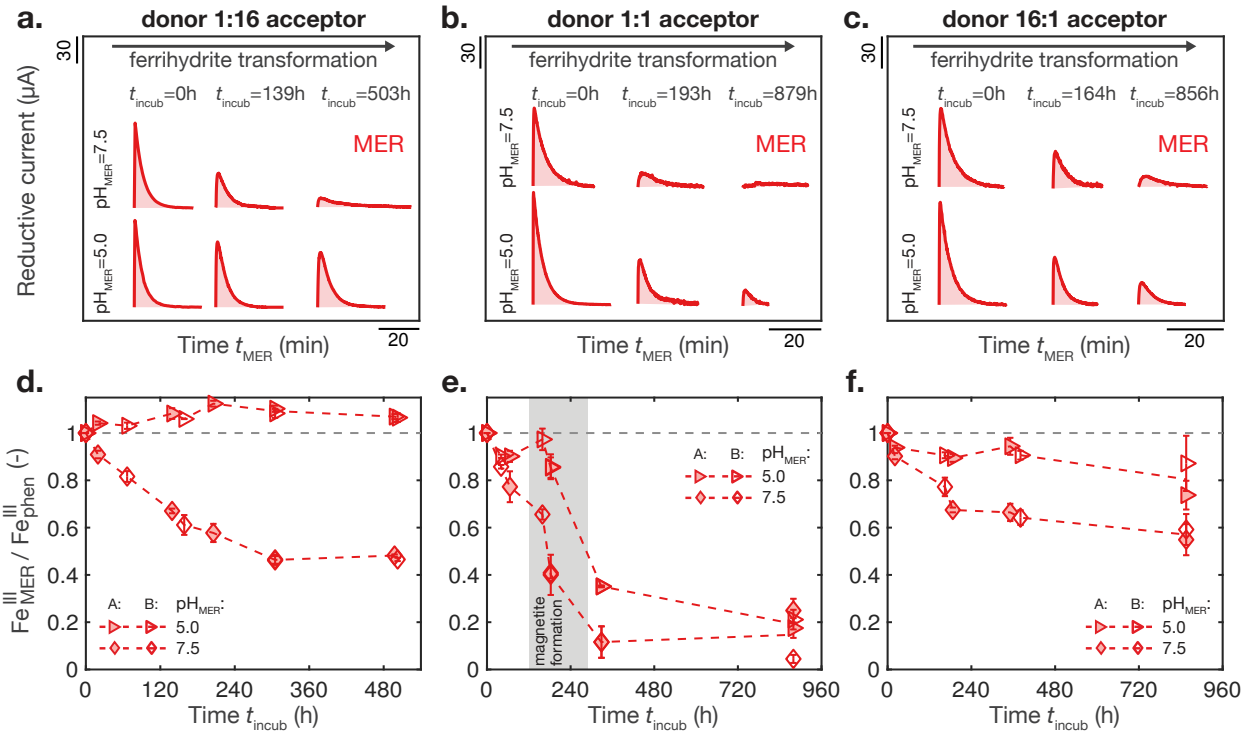

Figure 3. Changes in iron oxide reducibility over the course of the incubations as assessed by mediated electrochemical reduction (MER). Incubations were performed with 5.0 mM initial ferrihydrite-Fe^{III} and at initial electron donor-to-acceptor ratios in electron equivalents of 1:16 (panels a., d.), 1:1 (panels b., e.), and 16:1 (panels c., f.). MER data are shown for duplicate incubation vials (A and B in filled and open symbols, respectively). **a.-c.** Selected reductive current responses obtained during MER of iron oxide suspensions collected from the incubation vials at the beginning, at an intermediate time, and toward the end of the incubations, as specified on the plots. The x axis label t_{MER} refers to the time (min) during MER measurements. The horizontal scale bar next to the axis label depicts a time span of 20 min. Current responses were obtained in MER at pH_{MER}=5.0 (replotted from Figure 2a-c) and 7.5, both at applied reduction potentials of $E_H^{MER} = -0.35$ V. **d.-f.** Changes in iron oxide reducibility expressed in terms of reduction extents over the course of the incubations. Results of MER measurements at pH_{MER} = 7.5 (diamonds) and 5.0 (triangles) are shown. Reduction extents are presented as fractions of total oxide-Fe^{III} reducible in MER (i.e., $Fe^{III}_{MER}/Fe^{III}_{phen}$). Fe^{III}_{phen} was determined with the phenanthroline assay (phen). We ascribe the $Fe^{III}_{MER}/Fe^{III}_{phen}$ ratios > 1 in panel d to slightly lower Fe^{III} concentrations measured by the phenanthroline assay (Fe^{III}_{phen}) than actual Fe^{III} concentrations. This explanation is supported by the slightly incomplete mass balance in Figure 1a. The vertical grey bar in panel e. depicts the time span of magnetite formation. Lines in panels d.-f. serve as visual guides.

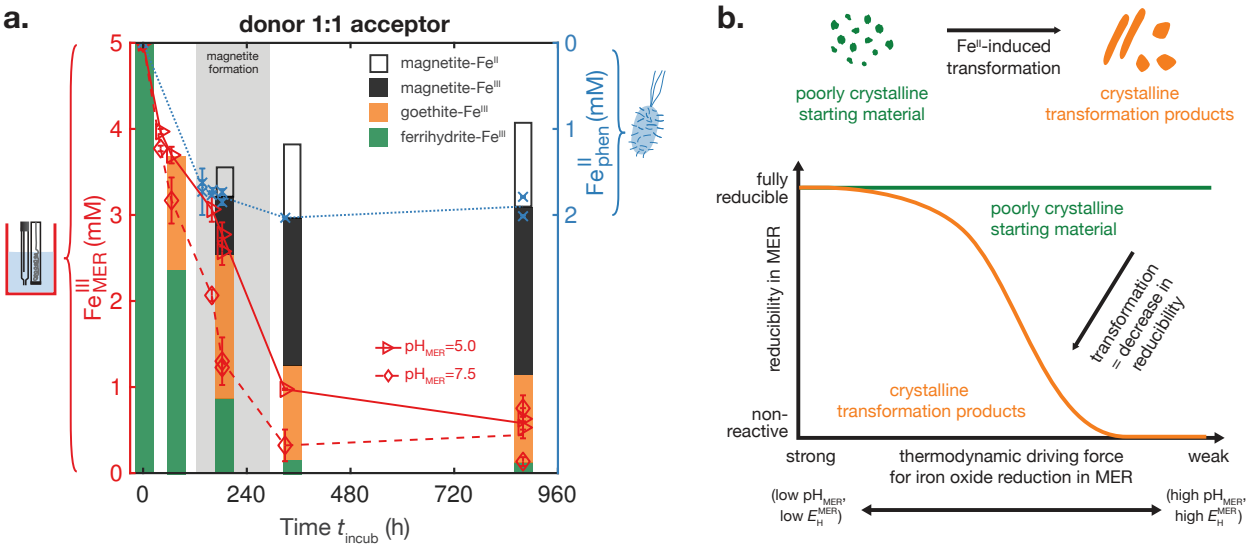

Figure 4. **a.** Combined analyses of microbial Fe^{III} reduction, iron oxide transformation, and decreases in iron oxide reducibility over the course of the incubation at an initial electron donor-to-acceptor ratio in electron equivalents of 1:1. Concentrations of Fe^{II}_{phen} are shown the right y axis (blue dotted line; determined by the phenanthroline assay and re-plotted from Figure 1b). Concentrations of Fe^{III}_{MER} at pH_{MER} = 5.0 (red triangles) and pH_{MER}=7.5 (red diamonds), both at applied reduction potentials of E_H^{MER} = −0.35 V, are shown on the left y axis. The concentration equivalents of Fe^{III} in ferrihydrite, goethite and magnetite were determined based on the molar Fe^{III} fractions in these iron oxides (Figure 1e) and are shown as colored stacked bars in green, orange and black, respectively. The concentration equivalents of Fe^{II} in magnetite were determined based on the molar Fe^{III} fraction in magnetite and the stoichiometry of magnetite and are shown as white bars. **b.** Schematic illustration of changes in iron oxide reducibility during the Fe^{II}-induced transformation of a poorly crystalline starting phase (green) into a (mixture of) crystalline transformation product(s) (orange). Iron oxide reducibility is determined in MER over a range of thermodynamic driving forces for iron oxide reductive dissolution, which can be altered by varying pH_{MER} and/or the applied reduction potential, E_H^{MER}.

Acknowledgement

The authors thank Kurt Barmettler for technical support and the Swiss National Science Foundation (SNF) for financial support (grant no. 200021_149283).

Supporting Information Available

The chemicals used in this study, the protocol for ferrihydrite synthesis, a description of the preparation of bacterial cultures, results of an exemplary sterile control experiment, results of additional experiments with bicarbonate and piperazine-1,4-bis(2-ethanesulfonic acid) buffers, details on X-ray diffraction analysis, X-ray diffractograms, details on electron microscopy investigations, description of the electrochemical cell setup, the Matlab code used for current peak analysis, results of experiments run at intermediate initial donor-to-acceptor ratios of 1:4 and 4:1, an overview of ferrous iron production and mineralogical transformation across all initial donor-to-acceptor ratios, exemplary electron microscopy images, data on magnetite stoichiometry, selected current responses in MER, and details on the calculation of reduction thermodynamics in MER. This material is available free of charge via the Internet at `http://pubs.acs.org/`.

References

(1) Raiswell, R.; Canfield, D. E. The iron biogeochemical cycle past and present. *Geochem. perspect.* **2012**, *1*, 1–220.

(2) Konhauser, K. O.; Kappler, A.; Roden, E. E. Iron in microbial metabolisms. *Elements* **2011**, *7*, 89–93.

(3) Taylor, K. G.; Konhauser, K. O. Iron in earth surface systems: A major player in chemical and biological processes. *Elements* **2011**, *7*, 83–88.

(4) Ehrlich, H. L.; Newman, D. K.; Kappler, A. In *Ehrlich's Geomicrobiology, Sixth Edition*; Ehrlich, H., Newman, D., Kappler, A., Eds.; CRC Press, 2015.

(5) Lovley, D. R. In *The Prokaryotes*; Rosenberg, E., DeLong, E. F., Lory, S., Stackebrandt, E., Thompson, F., Eds.; Springer Berlin Heidelberg: Berlin, Heidelberg, 2013; pp 287–308.

(6) Roden, E. E. Microbial iron-redox cycling in subsurface environments. *Biochem. Soc. Trans.* **2012**, *40*, 1249–1256.

(7) Weber, K. A.; Achenbach, L. A.; Coates, J. D. Microorganisms pumping iron: anaerobic microbial iron oxidation and reduction. *Nat. Rev. Microbiol.* **2006**, *4*, 752–764.

(8) Nealson, K. H.; Saffarini, D. Iron and manganese in anaerobic respiration: Environmental significance, physiology, and regulation. *Annu. Rev. Microbiol.* **2003**, *48*, 311–343.

(9) Phillips, E. J.; Lovley, D. R.; Roden, E. E. Composition of non-microbially reducible Fe(III) in aquatic sediments. *Appl. Environ. Microbiol.* **1993**, *59*, 2727–2729.

(10) Lovley, D. R. In *Iron Biominerals*; Frankel, R. B., Blakemore, R. P., Eds.; Springer, Boston, MA: New York, 1990; pp 151–166.

(11) Lovley, D. R.; Phillips, E. J. Availability of ferric iron for microbial reduction in bottom sediments of the freshwater tidal Potomac river. *Appl. Environ. Microbiol.* **1986**, *52*, 751–757.

(12) Cornell, R. M.; Schwertmann, U. *The Iron Oxides: Structure, Properties, Reactions, Occurrences and Uses*, 2nd ed.; Second, Completely Revised and Extended Edition; Wiley-VCH Verlag: Weinheim, 2003.

(13) Childs, C. W. Ferrihydrite: A review of structure, properties and occurrence in relation to soils. *Z. Pflanzenernähr. Bodenkd.* **1992**, *155*, 441–448.

(14) Hansel, C. M.; Benner, S. G.; Neiss, J.; Dohnalkova, A. C.; Kukkadapu, R. K.; Fendorf, S. Secondary mineralization pathways induced by dissimilatory iron reduction of ferrihydrite under advective flow. *Geochim. Cosmochim. Acta* **2003**, *67*, 2977–2992.

(15) Zachara, J. M.; Kukkadapu, R. K.; Fredrickson, J. K.; Gorby, Y. A.; Smith, S. C. Biomineralization of poorly crystalline Fe(III) oxides by dissimilatory metal reducing bacteria (DMRB). *Geomicrobiol. J.* **2002**, *19*, 179–207.

(16) Fredrickson, J. K.; Zachara, J. M.; Kennedy, D. W.; Dong, H.; Onstott, T. C.; Hinman, N. W.; Li, S.-m. Biogenic iron mineralization accompanying the dissimilatory reduction of hydrous ferric oxide by a groundwater bacterium. *Geochim. Cosmochim. Acta* **1998**, *62*, 3239–3257.

(17) Bonneville, S.; Behrends, T.; Van Cappellen, P. Solubility and dissimilatory reduction kinetics of iron(III) oxyhydroxides: A linear free energy relationship. *Geochim. Cosmochim. Acta* **2009**, *73*, 5273–5282.

(18) Cutting, R. S.; Coker, V. S.; Fellowes, J. W.; Lloyd, J. R.; Vaughan, D. J. Mineralogical and morphological constraints on the reduction of Fe(III) minerals by *Geobacter sulfurreducens*. *Geochim. Cosmochim. Acta* **2009**, *73*, 4004–4022.

(19) Roden, E. E. Geochemical and microbiological controls on dissimilatory iron reduction. *C. R. Geosci.* **2006**, *338*, 456–467.

(20) Bonneville, S.; Van Cappellen, P.; Behrends, T. Microbial reduction of iron(III) oxyhydroxides: effects of mineral solubility and availability. *Chem. Geol.* **2004**, *212*, 255–268.

(21) Roden, E. E. Fe(III) oxide reactivity toward biological versus chemical reduction. *Environ. Sci. Technol.* **2003**, *37*, 1319–1324.

(22) Roden, E. E.; Zachara, J. M. Microbial reduction of crystalline iron(III) oxides: Influence of oxide surface area and potential for cell growth. *Environ. Sci. Technol.* **1996**, *30*, 1618–1628.

(23) Borch, T.; Kretzschmar, R.; Kappler, A.; Van Cappellen, P.; Ginder-Vogel, M.; Voegelin, A.; Campbell, K. Biogeochemical redox processes and their impact on contaminant dynamics. *Environ. Sci. Technol.* **2010**, *44*, 15–23.

(24) Lovley, D. R.; Holmes, D. E.; Nevin, K. P. Dissimilatory Fe(III) and Mn(IV) reduction. *Adv. Microb. Physiol.* **2004**, *49*, 219–286.

(25) Thamdrup, B. In *Advances in Microbial Ecology*; Schink, B., Ed.; Springer, Boston, MA: Boston, MA, 2000; pp 41–84.

(26) Xiao, W.; Jones, A. M.; Li, X.; Collins, R. N.; Waite, T. D. Effect of *Shewanella oneidensis* on the kinetics of Fe(II)-catalyzed transformation of ferrihydrite to crystalline iron oxides. *Environ. Sci. Technol.* **2018**, *52*, 114–123.

(27) Xiao, W.; Jones, A. M.; Collins, R. N.; Bligh, M. W.; Waite, T. D. Use of fourier transform infrared spectroscopy to examine the Fe(II)-Catalyzed transformation of ferrihydrite. *Talanta* **2017**, *175*, 30–37.

(28) Perez-Gonzalez, T.; Jimenez-Lopez, C.; Neal, A. L.; Rull-Perez, F.; Rodriguez-Navarro, A.; Fernandez-Vivas, A.; Iañez-Pareja, E. Magnetite biomineralization induced by *Shewanella oneidensis*. *Geochim. Cosmochim. Acta* **2010**, *74*, 967–979.

(29) Hansel, C. M.; Benner, S. G.; Nico, P.; Fendorf, S. Structural constraints of ferric (hydr)oxides on dissimilatory iron reduction and the fate of Fe(II). *Geochim. Cosmochim. Acta* **2004**, *68*, 3217–3229.

(30) Fredrickson, J. K.; Kota, S.; Kukkadapu, R. K.; Liu, C.; Zachara, J. M. Influence of electron donor/acceptor concentrations on hydrous ferric oxide (HFO) bioreduction. *Biodegradation* **2003**, *14*, 91–103.

(31) Larsen, O.; Postma, D. Kinetics of reductive bulk dissolution of lepidocrocite, ferrihydrite, and goethite. *Geochim. Cosmochim. Acta* **2001**, *65*, 1367–1379.

(32) Postma, D. The reactivity of iron oxides in sediments: A kinetic approach. *Geochim. Cosmochim. Acta* **1993**, *57*, 5027–5034.

(33) Suter, D.; Banwart, S.; Stumm, W. Dissolution of hydrous iron(III) oxides by reductive mechanisms. *Langmuir* **1991**, *7*, 809–813.

(34) Dos Santos Afonso, M.; Morando, P. J.; Blesa, M. A.; Banwart, S.; Stumm, W. The reductive dissolution of iron oxides by ascorbate: The role of carboxylate anions in accelerating reductive dissolution. *J. Colloid Interface Sci.* **1990**, *138*, 74–82.

(35) Banwart, S.; Davies, S.; Stumm, W. The role of oxalate in accelerating the reductive dissolution of hematite (α-Fe_2O_3) by ascorbate. *Colloids Surf.* **1989**, *39*, 303–309.

(36) Aeppli, M.; Kaegi, R.; Kretzschmar, R.; Voegelin, A.; Hofstetter, T. B.; Sander, M. Electrochemical Analysis of Changes in Iron Oxide Reducibility during Abiotic Ferrihydrite Transformation into Goethite and Magnetite. *Environ. Sci. Technol.* **2019**, *53*, 3568–3578.

(37) Aeppli, M.; Voegelin, A.; Gorski, C. A.; Hofstetter, T. B.; Sander, M. Mediated electrochemical reduction of iron (oxyhydr-)oxides under defined thermodynamic boundary conditions. *Environ. Sci. Technol.* **2018**, *52*, 560–570.

(38) Sander, M.; Hofstetter, T. B.; Gorski, C. A. Electrochemical analyses of redox-active iron minerals: A review of nonmediated and mediated approaches. *Environ. Sci. Technol.* **2015**, *49*, 5862–5878.

(39) Aeschbacher, M.; Sander, M.; Schwarzenbach, R. P. Novel electrochemical approach to assess the redox properties of humic substances. *Environ. Sci. Technol.* **2010**, *44*, 87–93.

(40) Aeschbacher, M.; Graf, C.; Schwarzenbach, R. P.; Sander, M. Antioxidant properties of humic substances. *Environ. Sci. Technol.* **2012**, *46*, 4916–4925.

(41) Schwertmann, U.; Cornell, R. M. *Iron Oxides in the Laboratory: Preparation and Characterization*; Wiley-VCH, 2000.

(42) Stucki, J. W.; Anderson, W. L. The quantitative assay of minerals for Fe^{2+} and Fe^{3+} using 1,10-phenanthroline: I. Sources of variability. *Soil Sci. Soc. Am. J.* **1981**, *45*, 633–637.

(43) Tamura, H.; Goto, K.; Yotsuyanagi, T.; Nagayama, M. Spectrophotometric determination of iron(II) with 1,10-phenanthroline in the presence of large amounts of iron(III). *Talanta* **1974**, *21*, 314–318.

(44) ThomasArrigo, L. K.; Byrne, J. M.; Kappler, A.; Kretzschmar, R. Impact of organic matter on iron(II)-catalyzed mineral transformations in ferrihydrite–organic matter coprecipitates. *Environ. Sci. Technol.* **2018**, *52*, 12316–12326.

(45) Scarlett, N. V. Y.; Madsen, I. C. Quantification of phases with partial or no known crystal structures. *Powder Diffr.* **2006**, *21*, 278–284.

(46) Jaisi, D. P.; Dong, H.; Liu, C. Influence of biogenic Fe(II) on the extent of microbial reduction of Fe(III) in clay minerals nontronite, illite, and chlorite. *Geochim. Cosmochim. Acta* **2007**, *71*, 1145–1158.

(47) Jaisi, D. P.; Dong, H.; Liu, C. Kinetic analysis of microbial reduction of Fe(III) in nontronite. *Environ. Sci. Technol.* **2007**, *41*, 2437–2444.

(48) Mann, S.; Sparks, N. H. C.; Couling, S. B.; Larcombe, M. C.; Frankel, R. B. Crystallochemical characterization of magnetic spinels prepared from aqueous solution. *J. Chem. Soc., Faraday Trans. 1* **1989**, *85*, 3033–3044.

(49) Ardizzone, S.; Formaro, L. Temperature induced phase transformation of metastable $Fe(OH)_3$ in the presence of ferrous ions. *Mater. Chem. Phys.* **1983**, *8*, 125–133.

(50) Gorski, C. A.; Scherer, M. M. Determination of nanoparticulate magnetite stoichiometry by Mössbauer spectroscopy, acidic dissolution, and powder X-ray diffraction: A critical review. *Am. Mineral.* **2010**, *95*, 1017–1026.

(51) Cornell, R. M. Influence of organic anions on the crystallization of ferrihydrite. *Clays Clay Miner.* **1979**, *27*, 402–410.

(52) Tronc, E.; Belleville, P.; Jolivet, J. P.; Livage, J. Transformation of ferric hydroxide into spinel by iron(II) adsorption. *Langmuir* **1992**, *8*, 313–319.

(53) Gorski, C. A.; Nurmi, J. T.; Tratnyek, P. G.; Hofstetter, T. B.; Scherer, M. M. Redox behavior of magnetite: Implications for contaminant reduction. *Environ. Sci. Technol.* **2010**, *44*, 55–60.

(54) White, A. F.; Peterson, M. L.; Hochella Jr., M. F. Electrochemistry and dissolution kinetics of magnetite and ilmenite. *Geochim. Cosmochim. Acta* **1994**, *58*, 1859–1875.

(55) Stockbridge, C. D.; Sewell, P. B.; Cohen, M. Cathodic behavior of iron single crystals and the oxides Fe_3O_4, gamma−Fe_2O_3, and alpha−Fe_2O_3. *J. Electrochem. Soc.* **1961**, *108*, 928–933.

(56) Byrne, J. M.; Muhamadali, H.; Coker, V. S.; Cooper, J.; Lloyd, J. R. Scale-up of the production of highly reactive biogenic magnetite nanoparticles using *Geobacter sulfurreducens*. *J. Royal Soc. Interface* **2015**, *12*, 1–10.

(57) Carvallo, C.; Sainctavit, P.; Arrio, M. A.; Menguy, N.; Wang, Y.; Ona-Nguema, G.; Brice-Profeta, S. Biogenic vs. abiogenic magnetite nanoparticles: A XMCD study. *Am. Mineral.* **2008**, *93*, 880–885.

(58) Coker, V. S.; Pearce, C. I.; Lang, C.; van der Laan, G.; Pattrick, R. A. D.; Telling, N. D.; Schüler, D.; Arenholz, E.; Lloyd, J. R. Cation site occupancy of biogenic magnetite compared

to polygenic ferrite spinels determined by X-ray magnetic circular dichroism. *Eur. J. Mineral.* **2007**, *19*, 707–716.

(59) Gorski, C. A.; Edwards, R.; Sander, M.; Hofstetter, T. B.; Stewart, S. M. Thermodynamic characterization of iron oxide-aqueous Fe^{2+} redox couples. *Environ. Sci. Technol.* **2016**, *50*, 8538–8547.

(60) Fischer, W. R. Standard potentials (E_0) of iron(III) oxides under reducing conditions. *Z. Pflanzenernähr. Bodenkd.* **1987**, *150*, 286–289.

(61) Kluepfel, L. E.; Piepenbrock, A.; Kappler, A.; Sander, M. Humic substances as fully regenerable electron acceptors in recurrently anoxic environments. *Nature Geosci.* **2014**, *7*, 195–200.

(62) Watson, V. J.; Logan, B. E. Power production in MFCs inoculated with *Shewanella oneidensis* MR-1 or mixed cultures. *Biotechnol. Bioeng.* **2010**, *105*, 489–498.

(63) Borch, T.; Masue, Y.; Kukkadapu, R. K.; Fendorf, S. Phosphate imposed limitations on biological reduction and alteration of ferrihydrite. *Environ. Sci. Technol.* **2007**, *41*, 166–172.

(64) Hansel, C. M.; Learman, D. R.; Lentini, C. J.; Ekstrom, E. B. Effect of adsorbed and substituted Al on Fe(II)-induced mineralization pathways of ferrihydrite. *Geochim. Cosmochim. Acta* **2011**, *75*, 4653–4666.

(65) Ekstrom, E. B.; Learman, D. R.; Madden, A. S.; Hansel, C. M. Contrasting effects of Al substitution on microbial reduction of Fe(III) (hydr)oxides. *Geochim. Cosmochim. Acta* **2010**, *74*, 7086–7099.

636 # Graphical TOC Entry

637